High-energy neutron emission in thermal neutron-induced fission of ^{235}U

Martin Schulc [1], Michal Kostal [1], Roberto Capote [2], Jan Simon [1], Evzen Novak,[1] and Tomas Czakoj [1]
[1]*Research Centre Rez, Husinec-Rez 130, 250 68, Czech Republic*
[2]*NAPC–Nuclear Data Section, International Atomic Energy Agency, A-1400 Vienna, Austria*

(Received 7 December 2023; revised 19 March 2024; accepted 25 April 2024; published 20 May 2024; corrected 24 June 2024)

Spectrum-averaged cross-section (SACS) ratio measurement showing reduced uncertainties of measured SACS in two independent fission neutron fields is presented. The used prompt fission neutron fields correspond to the ^{252}Cf(sf) and ^{235}U($n_{\rm th}$, f) fission neutrons. The employed SACS in the ^{235}U($n_{\rm th}$, f) prompt fission neutron spectrum (PFNS) were measured using three different light water reactors: LR-0 and VR-1 zero power reactors and the LVR-15 10 MWt reactor. The employed SACS in the ^{252}Cf(sf) prompt fission neutron field were measured using a certified high-flux neutron source. Existing correlations among measured SACS in the two different neutron fields are estimated and used to reduce the uncertainty of measured SACS ratio for IRDFF dosimetry reactions. The derived set of measured SACS ratios with reduced uncertainty extends previous works into the higher-energy fission neutron range up to 20–30 MeV. The SACS ratio in ^{252}Cf(sf) and ^{235}U($n_{\rm th}$, f) PFNS can be used to probe the high-energy tail of the ^{235}U($n_{\rm th}$, f) fission neutron spectrum as the ^{252}Cf(sf) reference neutron spectrum is relatively well known. Derived experimental SACS ratio data. featuring low uncertainty are compared to the calculated dosimetry SACS ratio using the IRDFF-II dosimetry cross sections and the ^{235}U($n_{\rm th}$, f) ENDF/B-VII.1, ENDF/B-VIII.0, or JEFF-3.3 PFNS evaluations. The ENDF/B-VIII.0 evaluation of the ^{235}U($n_{\rm th}$, f) PFNS agrees well with derived SACS ratio data within quoted uncertainties. Other libraries predict a significantly lower fraction of ^{235}U($n_{\rm th}$, f) fission neutrons above 11 MeV of the outgoing neutron energy.

DOI: 10.1103/PhysRevC.109.054616

I. INTRODUCTION

Knowledge of the emitted fission neutrons contributes to the fundamental understanding of the fission process and fission dynamics. Fission neutrons play a major role in development of nuclear reactors and transmutation of used fuel [1]. These applications require a very accurate knowledge of the neutron multiplicity and of the prompt fission neutron spectrum (PFNS). PFNS early studies go back to 1939 before the Manhattan project [2]. After early qualitative discussions on PFNS by Zinn, Szilard, von Halban, Joliot, and Kowarski, and Bohr and Wheeler, Norman Feather of Cambridge was the first who provided a quantitative treatment of the neutron emission process during fission [3,4]. Feather correctly modeled the neutron emission process as the compound nucleus evaporation of neutrons from excited fast-moving fission fragments that are boosted by the fragment's motion.

The concept of scission neutrons can be also found in the 1942 Feather paper [4], which states "...concerning these secondary neutrons the general assumption has been that they are emitted within a short time of the formation of the unstable compound nucleus which results from the capture of the primary neutron *either before this nucleus divides*, or, more probably, from one or both of the fragment nuclei" (our highlight). This additional neutron emission mechanism during fission was also suggested by Fuller [5]. The scission neutron idea has been developed quantitatively in a quantum-mechanical microscopic frame by several authors [6–10]. Today we estimate that a minor fraction of fission neutrons may be emitted at the time of scission during fragments separation [7–11]—these neutrons are called scission neutrons and their energy spectrum is still an open question. Authors of Ref. [10] suggest the higher-energy scission spectrum compared to the typical neutron evaporation spectrum.

It is worth mentioning that all currently used fission theories and models for data evaluation are based on the assumption that fission neutrons are emitted from fission fragments by evaporation. However, the probability of neutron evaporation for neutrons with energies above 10 MeV is expected to be very small. Therefore, evaporation from fragments seldom can describe a significant amount of high-energy neutrons. Note that the small fraction of high-energy neutrons above 10 MeV (which is less than 3% of the total neutron flux) makes very difficult to obtain accurate experimental data in a given neutron field. This represents a challenge in using experimental PFNS data to discriminate between existing evaluated data libraries. The uncertainty of the evaluated PFNS of ^{252}Cf(sf) reaches about 20% at 10 MeV. Estimated PFNS uncertainties of high-energy neutrons for thermal-neutron-induced fission of fissile actinides are even larger, as the neutron multiplicity in ^{252}Cf(sf) of 3.7 is 30% larger than the 2.5 multiplicity observed for thermal-neutron-induced fission of ^{235}U.

Integral measurements of spectrum-averaged cross-section (SACS) ratio in ^{252}Cf(sf) and ^{235}U($n_{\rm th}$, f) neutron fields can be used as a probe to test the high-energy fission

neutron spectrum as they are only sensitive to the integral over the outgoing neutron flux above the corresponding dosimetry reaction threshold. However, the large PFNS uncertainty at high energies still has a large impact on the estimated SACS uncertainty in a given high-energy neutron field. The SACS ratio in two different neutron fields measured with lower uncertainty for high-threshold $(n, 2n)$ or $(n, 3n)$ dosimetry reactions has a clear advantage to be used as a spectrum probe. Therefore, if SACS ratio in ^{252}Cf(sf) and ^{235}U($n_{\rm th}$, f) neutron fields can be estimated with low uncertainty for high-energy threshold reactions, it will give a solid constraint to check the evaluated ^{235}U($n_{\rm th}$,f) neutron field assuming we know well the ^{252}Cf(sf) PFNS.

All presented SACS and its ratios were measured under the same conditions and using the same gamma spectrometer. The SACS is an integral quantity measured by activation with relatively low uncertainty, usually lower than 5%. We have employed a Monte Carlo method to estimate the correlations between the SACS measurements in two independent neutron fields. Such correlations may allow us to reduce the overall SACS ratio uncertainty, which allows us to discriminate between competing PFNS evaluations for high-energy neutrons. The presented SACS ratio set extends to much higher mean response energies (i.e., up to 26.5 MeV) than in previous works [12–19]. These data-set ratios use results previously published by our group [20–25].

The ^{235}U($n_{\rm th}$, f) PFNS evaluations in the major libraries significantly differ. The high-energy part of ENDF/B-VIII.0 ^{235}U($n_{\rm th}$, f) PFNS was obtained by adjusting the high-energy tail above 10 MeV to reproduce the experimental ^{90}Zr$(n, 2n)$ SACS [26–30]. Other evaluations used in this paper, i.e., the JEFF-3.3 [31] or the ENDF/B-VII.1 [32] evaluations, were based on the Los Alamos or Madland–Nix model [33].

This work is devoted to the analysis of previously performed SACS measurements in two different neutron fields. Using the well-known ^{252}Cf(sf) PFNS we expect to estimate the fraction of high-energy fission neutrons in thermal-neutron-induced fission of ^{235}U targets. The problem is discussed in the Introduction. Section II contains a brief description of the employed neutron sources for SACS measurements. Section III is devoted to the description of the experimental and theoretical methods. Section IV describes the SACS ratio methodology while Sec. V contains the SACS ratio uncertainty quantification. Results are presented and discussed in Sec. VI, while Sec. VII summarizes our findings and list the conclusions.

II. USED NEUTRON FACILITIES

The SACS measurements in different neutron fields have been previously published, but a summary of employed neutron sources is given below for completeness.

A. LR-0 reactor

The LR-0 research reactor is a zero-power light-water pool-type reactor. Experiments were performed at atmospheric pressure and at room temperature in a specially designed core assembled in the LR-0 reactor. This special core [34] consists of six uranium fuel assemblies with nearly 3.3% ^{235}U enrichment surrounding a special dry assembly which contains the activation foils in a sample holder. Used fuel assemblies are the same as VVER-1000 (water-water energetic reactor) type in radial direction but not in axial direction, whereas the fission column is shortened to 125 cm. Fuel assemblies have lattice pitch of 23.6 cm. Reactor criticality was achieved by change of a moderator level only (which is water). The special core was listed as a reference neutron field for the IRDFF-II nuclear data library testing [35]. The core was well characterized by reactivity experiments [36], fission rates distribution [37], and also neutron spectrum measurements in different material insertions in its center [38]. The details of SACS measurements in LR-0 can be found in Refs. [39–41].

B. VR-1 reactor

The VR-1 research reactor is also a light-water, zero-power pool-type reactor located in Prague. The core consists of tubular fuel assemblies of IRT-4M (tubular-type of the nuclear fuel, version 4M) type enriched to 19.75 wt.% of ^{235}U and contains several dry vertical channels with different diameters up to 90 mm and one radial channel with diameter of 250 mm. The activation targets were placed in the center of a 25-mm channel located in the center of fuel assembly positioned close to the radial channel of the reactor. Criticality of the reactor during irradiation was managed by movement of the control rods. The details of the experiments and SACS measurements can be found in Ref. [42].

C. LVR-15 reactor

The LVR-15 is a light-water moderated tank-type research reactor with a maximal possible thermal power of 10 MWt, forced cooling, water and/or beryllium reflector, and IRT-4M fuel with enrichment of 19.7% of ^{235}U. Due to the high operating powers the fuel has a burn-up and contains some plutonium. Fuel composition is assessed by means of calculations using an onsite developed code NODER [43]. Despite these circumstances, the measurement of SACS is possible near the fuel assemblies where a high flux of high-energy neutrons is achieved [20].

D. ^{252}Cf(sf) high-intensity source

The ^{252}Cf(sf) source involved in ^{252}Cf experiments was provided by Frontier Technology and had initial emission of $(9.53 \pm 0.11) \times 10^8$ n/s on August 13, 2015, at 12:00 GMT according to the data in the certificate of calibration involving manganese sulphate bath measurements performed at the National Physical Laboratory, UK. The current experiments were performed during source emission of roughly 8.0×10^8 n/s down to emission of 2.9×10^8 n/s. The ^{252}Cf(sf) source and irradiation geometry are well described and verified in Ref. [44]. Many experiments have been undertaken using this source and SACS measurements have been published in Refs. [21–25].

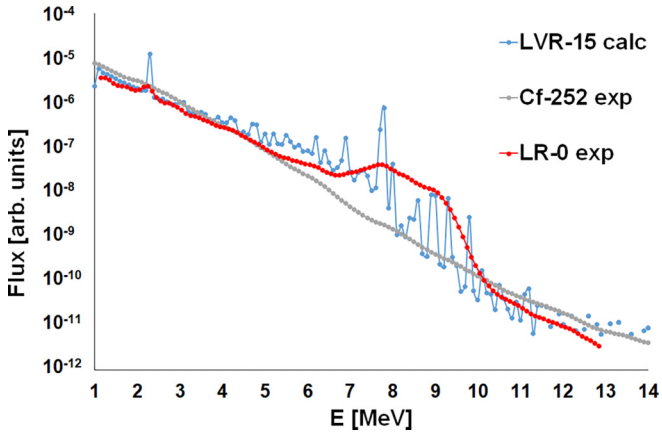

FIG. 1. Gamma spectra in different neutron fields.

E. Impact of photon-induced reactions on measured SACS

Some (γ, xn) photon-induced reactions lead to the same residual nucleus as the corresponding (n, xn) reactions, and therefore the impact of photon-induced reactions on measured SACS should be assessed. Figure 1 displays the measured γ spectrum in LR-0 reactor [45], measured ^{252}Cf prompt fission γ spectrum [46], and calculated γ spectrum for measurement position in LVR-15 reactor. The shape of the γ spectra below 5 MeV is similar for all neutron sources. We see a bump from 5 to 10 MeV of outgoing γs in reactor spectra, which is related to prompt capture γs from reactions on structural materials (which are missing for the Cf source). The influence of (γ, xn) reactions was estimated computationally using these γ spectra combined with the TENDL-2021 [47] γ interaction cross sections. The highest γ contribution of approximately $(1.8 \pm 0.9)\%$ was found for the reaction ^{197}Au$(n, 2n)^{196}$Au. This contribution has increased the uncertainty. Contributions to other dosimetry reactions were found to be under 0.8%, which is well within measurement uncertainties, and were neglected.

III. DESCRIPTION OF THE EXPERIMENTAL AND CALCULATION METHODS

All calculations to obtain SACS in a given neutron spectrum were performed using the MCNP6.2 transport code [48]. Cross sections of the dosimetry reactions under study were taken from the IRDFF-II library [35]. ^{252}Cf(sf) neutron spectrum based on Mannhart evaluation was taken from the IRDFF validation website [49]. The transport files employed in the transport and correction calculations were taken from the ENDF/B-VII.I library [32] except for ^{235}U which was taken alternatively from ENDF/B-VIII.0 library [26], ENDF/B-VII.1 library, or JEFF-3.3 [31] to show major differences in evaluated prompt fission thermal-neutron spectrum. ENDF/B-VII.I library was chosen for transport because of consistency with older calculations before the release of the ENDF/B-VIII.0 library.

The activation samples containing isotopes under study were either low volume or high volume. Low-volume samples were often placed on the upper cap of the coaxial high-purity germanium (HPGe) detector in a vertical configuration (ORTEC GEM35P4) to achieve reasonable statistics in a reasonable time. If the dead time of the detector was over 4%, then the samples were placed at the distance of 10–20 cm from the upper cap of the detector to eliminate the dead time. Corrections to the true summation were employed in cases where applicable [39]. High-volume samples were strewn into Marinelli beaker and homogenized after the irradiation to achieve a well-defined geometry and also better efficiency of the measuring geometry. Irradiations took from several hours to several months to shorten the γ-spectroscopy measurement time.

The crucial quantity affecting the results and their uncertainty is the efficiency of the germanium detector. The efficiencies were calculated in MCNP6.2 using experimentally validated mathematical model [39].

The experimental reaction rates were derived from the net peak areas measured using the semiconductor HPGe detector. These measured reaction rates were used to derive the SACS as described in the next section. A detailed description of the method can be found in Ref. [21]. The ^{235}U SACS were compiled from measurements using three different reactors, LR-0 reactor reference neutron field, LVR-15 reactor for higher fluxes needed to access high-energy regions, and VR-1 zero power reactor for intercomparison. The measurements were performed inside the reactors near the fuel rods. The influence of the neutron transport in water and surrounding structural materials on the ^{235}U PFNS was computationally found to have a negligible effect [34].

IV. SACS METHODOLOGY AND VALIDATION

As the irradiation of some of the activation foils was performed discontinuously, the evaluation of the reaction rate was performed using the following formula:

$$q(\bar{P}) = \frac{A(\bar{P})}{A_{\mathrm{Sat}}(\bar{P})} \frac{\mathrm{NPA}(T_m) C_{\mathrm{SCF}} \lambda}{N \epsilon \eta k} \frac{T_m}{T_l} \frac{1}{1 - \exp(-\lambda T_m)} \times \frac{1}{\exp(-\lambda \Delta T)}, \quad (1)$$

where N is the number of target isotope nuclei, η is the detector efficiency, ϵ is the γ branching ratio, λ is the decay constant, C_{SCF} is the coincidence correction factor, k characterizes the abundance of the isotope of interest in the target and its purity, ΔT is the cooling time between the end of irradiation and the start of HPGe measurement, $\mathrm{NPA}(T_m)$ is the measured net peak area, T_m is the real time of measurement by HPGe, T_l is the live time of measurement by HPGe (it is time of measurement corrected to the dead time of the detector), $q(\bar{P})$ is the reaction rate of activation during different neutron source emission $(\bar{P})$, and $\frac{A(\bar{P})}{A_{\mathrm{Sat}}}$ corresponds to the inverted relative portion of the saturated activity induced during the experiment. This fraction is crucial in the case of interrupted irradiations or irradiations with varying neutron emission.

The experimental SACS are then derived from the measured reaction rate as follows: the experimental reaction rate is multiplied by the correction factor C calculated in MCNP6 to take into account the spectrum shift effect, flux loss, and

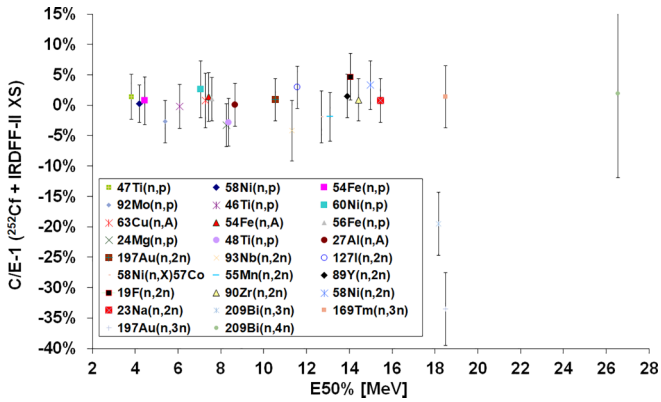

FIG. 2. Calculation to experiment (C/E) ratio for SACS of dosimetry reactions in the ^{252}Cf(sf) reference neutron field as a function of the mean response neutron energy $E50\%$.

self-shielding together. It is a ratio between the spectrum-averaged cross section in the real geometry and the spectrum-averaged cross section in the geometrically identical setup but consisting of void cells. The resulting SACS are derived using the following equation:

$$\bar{\sigma} = \frac{q \times C}{\int_0^{+\infty} \Phi(E) dE}, \tag{2}$$

where C denotes the correction factor, $\Phi(E)$ is the calculated neutron spectrum, $\bar{\sigma}$ is the spectrum-averaged cross section, and q is the measured reaction rate.

Figure 2 shows the calculated (C) to experiment (E) SACS ratio in the ^{252}Cf(sf) reference neutron field. Calculated SACS used the IRDFF-II dosimetry cross sections (C) combined with the IRDFF-II ^{252}Cf(sf) reference neutron field to estimate the (C) SACS compared to the experimentally derived SACS (E) for 26 dosimetry reactions. The obtained C/E agreement is within uncertainties for all selected dosimetry reactions, except for Au$(n, 3n)$ and Bi$(n, 3n)$ reactions, over a broad mean response neutron energy range $E50\%$. $E50\%$ is the neutron energy which corresponds to a 50% value of the integrated energy response function in the neutron field, i.e., is the mean neutron energy response. Since ^{252}Cf(sf) is a neutron standard spectrum, the 24 studied cross sections with C/E within uncertainties were validated. The cross section of ^{58}Ni$(n, X)^{57}$Co were taken from the ENDF/B-VIII.0 library, all other cross sections were taken from the IRDFF-II library.

V. UNCERTAINTY EVALUATION

The SACS experimental uncertainty budget includes the counting rate uncertainties in HPGe detector, the detector efficiency uncertainty, uncertainties in the sample position during irradiation, uncertainties in the emission (reactor power) of the neutron source, and uncertainties of the correction factor. Other sources of uncertainty were neglected. The detailed information concerning uncertainty budget for individual experiments can be found in previously published papers [20–25,39–42].

To estimate the SACS ratio uncertainty, the approach to lower the resulting uncertainty is based on the fact that some of the quantities defining the SACS measured in different neutron fields are strongly correlated. This is especially true for the efficiency of the HPGe detector (note that the same detector is used to measure the selected reaction in both neutron fields.), which is loaded with systematic uncertainty and directly correlated with the resulting SACS value. Note that the same HPGe detector is used to measure the selected reaction in both neutron fields. The irradiated samples were similar for both neutron fields, i.e., the detector efficiency was very much the same. To lower the total uncertainty, correlations between SACS in different neutron fields corr$(\mathrm{SACS}_{235}, \mathrm{SACS}_{252})$ were calculated from the samples, and the ratio uncertainty $\Delta R/R$ is derived by means of Eq. (3):

$$\begin{aligned}\Delta R/R = \mathrm{sqrt}[&(\Delta_{252}/\mathrm{SACS}_{252})^2 + (\Delta_{235}/\mathrm{SACS}_{235})^2 \\ &- 2(\Delta_{252}/\mathrm{SACS}_{252})(\Delta_{235}/\mathrm{SACS}_{235}) \\ &\times \mathrm{corr}(\mathrm{SACS}_{252}, \mathrm{SACS}_{235})],\end{aligned} \tag{3}$$

where ΔR denotes the ratio final uncertainty; Δ_{252} and Δ_{235} are the SACS uncertainties in ^{252}Cf(sf) or ^{235}U neutron fields, respectively; and R is the SACS ratio. Ratio R is a function of the net peak area, live, real, and cooling time of measurements only. Other variables cancel out in the case of using the same sample and is described by Eq. (4),

$$R = \frac{\mathrm{NPA}_{252}}{\mathrm{NPA}_{235}} \frac{T_{m252}}{T_{m235}} \frac{T_{l235}}{T_{l252}} \frac{1 - \exp(-\lambda T_{m235})}{1 - \exp(-\lambda T_{m252})} \frac{\exp(-\lambda \Delta T_{235})}{\exp(-\lambda \Delta T_{252})}. \tag{4}$$

To determine the correlations, sets of 5000 SACS were generated for every reaction in both neutron fields using the experimental data, i.e. net peak areas, live, real, and cooling times. Due to the high number of counts in net peak areas, we assumed that net peak area uncertainty is distributed by normal distribution. Both the ^{235}U(n_{th}, f) and ^{252}Cf(sf) net peak areas sets were generated by the Monte Carlo method from the inverse error function involving experimentally estimated net peak areas using appropriate experimental uncertainties. Measurement times were considered as constants dependent on the appropriate reaction. Times were measured with very low uncertainties. The computed SACS correlations were positive in all cases, which led to much lower final uncertainty of the ratio compared to the independent estimate (zero correlations). Mean detector uncertainties in each neutron field and estimated numerator to the denominator correlations are listed in Table I for all reactions under study.

VI. RESULTS

Table II shows dosimetry reactions under study as a function of together of the mean neutron response energy $E50\%$ for the two neutron fields, the corresponding SACS ratio, and the estimated total uncertainty for the set of neutron-induced reactions in the broad range of mean response energies. The R ratio was experimentally measured from $E50\% = 3.73$ MeV to 26.54 MeV. Figure 3 shows the ^{252}Cf(sf) and ^{235}U(n_{th}, f) SACS ratios as a function of the mean neutron response energy of each dosimetry

TABLE I. Uncertainties ΔR of the SACS ratio R and estimated correlations corr($SACS_{252}$, $SACS_{235}$) for all reactions under study. ^{169}Tm$(n, 3n)$ was not measured in reactors.

Reaction	Δ_{235} (%)	Δ_{252} (%)	Correlation
^{47}Ti$(n, p)^{47}$Sc	2.8	3.7	0.69
^{58}Ni$(n, p)^{58}$Co	3.0	3.1	0.59
^{54}Fe$(n, p)^{54}$Mn	2.5	3.9	0.76
^{92}Mo$(n, p)^{92m1}$Nb	2.1	3.8	0.81
^{46}Ti$(n, p)^{46}$Sc	3.1	3.6	0.65
^{60}Ni$(n, p)^{60}$Co	4.6	4.8	0.61
^{63}Cu$(n, \alpha)^{60}$Co	3.4	4.5	0.70
^{54}Fe$(n, \alpha)^{51}$Cr	3.0	4.3	0.72
^{56}Fe$(n, p)^{56}$Mn	2.0	3.5	0.82
^{24}Mg$(n, p)^{24}$Na	2.1	3.5	0.79
^{48}Ti$(n, p)^{48}$S	2.9	3.9	0.69
^{27}Al$(n, \alpha)^{24}$Na	3.1	3.5	0.64
^{197}Au$(n, 2n)^{196}$Au	4.0	3.5	0.54
^{93}Nb$(n, 2n)^{92m1}$Nb	2.2	3.9	0.79
^{127}I$(n, 2n)^{126}$I	4.9	3.5	0.44
^{58}Ni$(n, X)^{57}$Co	5.6	3.6	0.41
^{55}Mn$(n, 2n)^{54}$Mn	2.9	4.0	0.74
^{89}Y$(n, 2n)^{88}$Y	3.7	3.7	0.71
^{19}F$(n, 2n)^{18}$F	2.5	3.8	0.74
^{90}Zr$(n, 2n)^{89}$Z	4.3	3.5	0.50
^{58}Ni$(n, 2n)^{57}$Ni	3.2	4.0	0.68
^{23}Na$(n, 2n)^{22}$Na	4.7	3.6	0.49
^{209}Bi$(n, 4n)^{206}$Bi	9.1	13.9	0.76

TABLE II. Mean response neutron energies in MeV for dosimetry reactions and corresponding experimental SACS ratios and their relative uncertainties. ^{169}Tm$(n, 3n)$ was not measured in reactors.

Reaction	$E50\%$ (MeV)	SACS Ratio	Unc. (%)
^{47}Ti$(n, p)^{47}$Sc	3.73	1.042	2.7
^{58}Ni$(n, p)^{58}$Co	4.12	1.088	2.8
^{54}Fe$(n, p)^{54}$Mn	4.36	1.056	2.6
^{92}Mo$(n, p)^{92m1}$Nb	5.29	1.170	2.4
^{46}Ti$(n, p)^{46}$Sc	5.98	1.273	2.9
^{60}Ni$(n, p)^{60}$Co	6.57	1.352	4.2
^{63}Cu$(n, \alpha)^{60}$Co	7.14	1.282	3.2
^{54}Fe$(n, \alpha)^{51}$Cr	7.31	1.327	3.0
^{56}Fe$(n, p)^{56}$Mn	7.46	1.367	2.2
^{24}Mg$(n, p)^{24}$Na	8.19	1.404	2.2
^{48}Ti$(n, p)^{48}$Sc	8.22	1.460	2.8
^{27}Al$(n, \alpha)^{24}$Na	8.56	1.454	2.8
^{197}Au$(n, 2n)^{196}$Au	10.47	1.686	3.7
^{93}Nb$(n, 2n)^{92m1}$Nb	11.26	1.872	2.5
^{127}I$(n, 2n)^{126}$I	11.51	1.715	4.6
^{58}Ni$(n, X)^{57}$Co	12.60	1.900	5.3
^{55}Mn$(n, 2n)^{54}$Mn	13.02	1.990	2.7
^{89}Y$(n, 2n)^{88}$Y	13.84	2.076	2.6
^{19}F$(n, 2n)^{18}$F	13.96	1.973	2.6
^{90}Zr$(n, 2n)^{89}$Zr	14.35	2.022	3.9
^{58}Ni$(n, 2n)^{57}$Ni	14.91	2.070	3.0
^{23}Na$(n, 2n)^{22}$Na	15.37	2.211	4.3
^{209}Bi$(n, 4n)^{206}$Bi	26.54	3.007	9.1

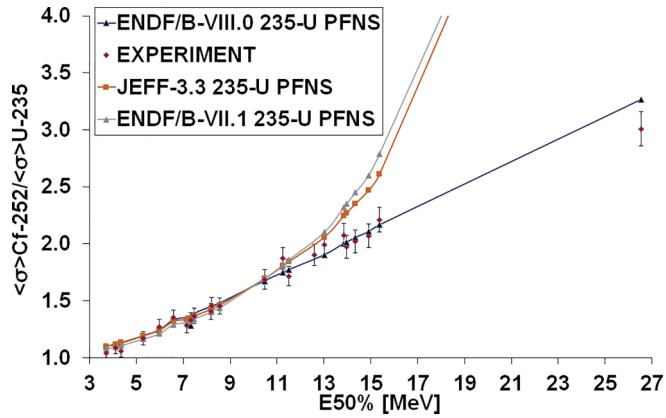

FIG. 3. SACS ratios and uncertainties as a function of the mean neutron response energy $E50\%$ of each dosimetry reaction listed in Table 2.

reaction. The experimental results agree very well with calculated SACS ratio data using the ^{235}U$(n_{\rm th}, f)$ ENDF/B-VIII.0 PFNS. If JEFF-3.3 and/or ENDF/B-VII.1 PFNS are used, then we see a lack of neutrons above 11 MeV connected to a much softer evaluated fission neutron spectrum. A new version of the ENDF/B library to be released in 2025 (the ENDF/B-VIII.1 library) contains the same ^{235}U$(n_{\rm th}, f)$ PFNS as in the ENDF/B-VIII.0 library. The experimental result shows the ratio of only 2.211 for $E50\% = 15.4$ MeV in excellent agreement with the ENDF/B-VIII.0 value, unlike the 2.60 value obtained for the JEFF-3.3 or 2.75 value for the ENDF/B-VII.1 libraries. The difference among different evaluations starts to be visible from approximately 11 MeV of outgoing neutron energy. The measured experimental ratio above 11 MeV contradicts current theoretical fission models where all fission neutrons come from fission fragments' evaporation spectrum. High-energy scission neutrons reported in Refs. [9,10] may explain the observed experimental trend. Further theoretical research is needed.

VII. SUMMARY AND CONCLUSIONS

A set of measured ^{252}Cf(sf) and ^{235}U$(n_{\rm th}, f)$ SACS ratios with low uncertainties is being derived in a broad range of mean response neutron energies. These data were used to test evaluated prompt fission neutron spectra of ^{235}U$(n_{\rm th}, f)$ assuming that the reference ^{252}Cf(sf) is well known. The measured SACS ratio data for mean neutron response energies above 11 MeV are very well reproduced within quoted uncertainties using the ENDF/B-VIII.0 ^{235}U$(n_{\rm th}, f)$ PFNS and Mannhart ^{252}Cf spontaneous fission neutron spectrum evaluations. The SACS calculated using the JEFF-3.3 and ENDF/B-VII.1 ^{235}U$(n_{\rm th}, f)$ PFNS do not agree with experimental data above the 11 MeV of neutron outgoing energy. The obtained SACS ratio data clearly shows that the ^{235}U$(n_{\rm th}, f)$ PFNS has neutrons with very high energy over 20 MeV. The presented data poses a serious challenge for dominant fission neutron emission models. We have experimentally established the existence of high-energy fission neutrons with

energies up to 30 MeV, the mechanism of their production cannot be established experimentally. A possible explanation could be the presence of high-energy scission neutrons. Further theoretical and experimental investigations are warranted. To measure SACS in a ^{235}U(n_{th}, f) neutron field outside a high-flux reactor core may help.

ACKNOWLEDGMENTS

The presented results were obtained using the CICRR infrastructure, which is financially supported by the Ministry of Education, Youth and Sports, Czech Republic (Ministerstvo kolství, mládee a tělovýchovy české republiky)- Project No. LM2023041.

[1] J. O. Denschlag, *Technical Application of Nuclear Fission* (Springer Science+Business, New York, 2011), pp. 2613–2661.
[2] M. B. Chadwick and R. Capote, Manhattan project 1940s research on the prompt fission neutron spectrum, Front. Phys. **11**, 1105593 (2023).
[3] N. Feather, The time involved in the process of nuclear fission, Nature **143**, 597 (1939).
[4] N. Feather, *Emission of Neutrons from Moving Fission Fragments*, Tech. Rep. Cambridge, U. S. Atomic Energy Commission Document No. BR 335A and British Mission BM-143 (United States Atomic Energy Commission Technical Information Division, ORE, Oak Ridge, Tennessee, 1942).
[5] R. Fuller, Dependence of neutron production in fission on rate of change of nuclear potential, Phys. Rev. **126**, 684 (1962).
[6] N. Carjan and P. Talou, and O. Serot, Emission of scission neutrons in the sudden approximation, Nucl. Phys. A **792**, 102 (2007).
[7] R. Capote, Y.-J. Chen, F.-J. Hambsch, N. V. Kornilov, J. P. Lestone, O. Litaize, B. Morillon, D. Neudecker, S. Oberstedt, T. Ohsawa, N. Otuka, V. G. Pronyaev, A. Saxena, O. Serot, O. A. Shcherbakov, N.-C. Shu, D. L. Smith, P. Talou, A. Trkov, A. C. Tudora, R. Vogt, and A. C. Vorobyev, Prompt fission neutron spectra of actinides, Nucl. Data Sheets **131**, 1 (2016).
[8] R. Capote, N. Carjan, and S. Chiba, Scission neutrons for U, Pu, Cm, and Cf isotopes: Relative multiplicities calculated in the sudden limit, Phys. Rev. C **93**, 024609 (2016).
[9] N. Carjan and M. Rizea, Structures in the energy distribution of the scission neutrons: Finite neutron-number effect, Phys. Rev. C **99**, 034613 (2019).
[10] I. Abdurrahman, M. Kafker, A. Bulgac, and I. Stetcu, Neck rupture and scission neutrons in nuclear fission, arXiv:2307.13132v2.
[11] N. V. Kornilov, F.-J. Hambsch, I. Fabry, S. Oberstedt, and S. P. Simakov, New experimental and theoretical results for the ^{235}U thermal fission neutron spectrum, in *International Conference on Nuclear Data for Science Technology* (CEA, EDP Sciences, France, 2008).
[12] K. Kobayashi and I. Kimura, Fission spectrum averaged cross sections with standard neutron fields, in *Proceedings of the 3rd ASTM-EURATOM Symposium on Reactor Dosimetry* (JRC Petten, Brussels, 1980), p. 1004.
[13] K. Kobayashi *et al.*, The ^{235}U fission neutron spectrum adjusted with multi-foil activation data, in *Proceedings of the Seventh ASTM-EURATOM Symposium on Reactor Dosimetry, Strasbourg* (Kluwer Academics, Brussels, 1992), p. 263.
[14] R. Capote *et al.*, Updating and extending the IRDF-2002 dosimetry library, J. ASTM Int. 9, 197 (2012) JAI104119 Data available online at https://www-nds.iaea.org/IRDFF/.
[15] K. I. Zolotarev, Re-evaluation of microscopic and integral cross-section data for important dosimetry reactions, Report INDC(NDS)-0526 (IAEA, Vienna, 2008).
[16] K. I. Zolotarev, Evaluation of cross section data from threshold to 40–60 MeV for specific neutron reactions important for neutron dosimetry applications, Report INDC(NDS)-0546 (IAEA, Vienna, 2009).
[17] K. I. Zolotarev, Evaluation of cross section data from threshold to 40 MeV for some neutron reactions important for fusion dosimetry applications, Report INDC(NDS)-0584 (IAEA, Vienna, 2010).
[18] W. Mannhart, Validation of differential cross sections with integral data, IAEA Technical Report INDC(NDS)-0435 (IAEA, Vienna, 2002), pp. 59–64.
[19] W. Mannhart, Status of the evaluation of the neutron spectrum of ^{252}Cf(sf), IAEA Technical Report INDC(NDS)-0540 (IAEA, Vienna, 2008).
[20] M. Schulc, M. Koštál, J. Šimon, F. Brijar, T. Czakoj, and J. P. Malý, Constraining high energy tail of ^{235}U(n_{th}, f) prompt fission neutron spectrum, Appl. Radiat. Isot. **166**, 109313 (2020).
[21] M. Schulc, M. Koštál, S. Simakov, V. Rypar, D. Harutyunyan, J. Šimon, N. Burianová, E. Novák, B. Jánský, M. Mareček *et al.*, Validation of differential cross sections by means of ^{252}Cf spectral averaged cross sections, Appl. Radiat. Isot. **132**, 29 (2018).
[22] M. Schulc, M. Koštál, R. Capote, E. Novák, J. Šimon, N. Burianová, and A. Wallner, Validation of selected (n, 2n) dosimetry reactions in IRDFF-1.05 library, Appl. Radiat. Isot. **143**, 132 (2019).
[23] M. Schulc, M. Koštál, E. Novák, J. Šimon, and N. Burianová, Investigation of ^{127}I(n, 2n)^{126}I and ^{23}Na(n, 2n)^{22}Na reactions using ^{252}Cf neutron source, ASME J. Nucl. Rad. Sc. **5**, 030918 (2019).
[24] M. Schulc, M. Koštál, J. Šimon, E. Novák, M. Mareček, and R. Kubín, Validation of IRDFF-II library by means of ^{252}Cf spectral averaged cross sections, Appl. Radiat. Isot. **155**, 108937 (2020).
[25] M. Schulc, M. Koštál, J. Šimon, E. Novák, V. Juříček, and M. Mareček, Measurement of very high threshold reactions using ^{252}Cf source, Appl. Radiat. Isot. **166**, 109355 (2020).
[26] D. A. Brown, M. B. Chadwick, R. Capote, A. C. Kahler, A. Trkov, M. W. Herman, A. A. Sonzogni, Y. Danon, A. D. Carlson, M. Dunn *et al.*, ENDF/B-VIII.0: The 8th major release of the nuclear reaction data library with CIELO-project cross sections, new standards and thermal scattering data, Nucl. Data Sheets, **148**, 1 (2018).
[27] R. Capote *et al.*, IAEA CIELO evaluation of neutron-induced reactions on ^{235}U and ^{238}U targets, Nucl. Data Sheets **148**, 254 (2018).
[28] A. Trkov and R. Capote, Evaluation of the prompt fission neutron spectrum of thermal-neutron induced fission in ^{235}U, Phys. Proc. **64**, 48 (2015).
[29] A. Trkov, R. Capote, and V. G. Pronyaev, Current issues in nuclear data evaluation methodology: ^{235}U(n_{th}, f) prompt fission

neutron spectra and multiplicity for thermal neutrons, Nucl. Data Sheets **123**, 8 (2015).
[30] N. Bohr, J. A. Wheeler, The mechanism of nuclear fission, Phys. Rev. **56**, 426 (1939).
[31] O. Cabellos *et al.*, Benchmarking and validation activities within JEFF project, EPJ Web Conf. **146**, 06004 (2017).
[32] M. B. Chadwick *et al.*, ENDF/B-VII.1: Nuclear data for science and technology: Cross sections, covariances, fission product yields and decay data, Nucl. Data Sheets **112**, 2887 (2011).
[33] D. G. Madland, J. R. Nix, New calculation of prompt fission neutron spectra and average prompt neutron multiplicities, Nucl. Sci. Eng. **81**, 213 (1982).
[34] M. Košťál *et al.*, A reference neutron field for measurement of spectrum averaged cross sections, Ann. Nucl. Energy **140**, 107119 (2020).
[35] A. Trkov *et al.*, IRDFF-II: A new neutron metrology library, Nucl. Data Sheets **163**, 1 (2020).
[36] M. Košťál *et al.*, Study of graphite reactivity worth on well-defined cores assembledon LR-0 reactor, Ann. Nucl. Energy. **87**, 601 (2016).
[37] M. Košťál *et al.*, Determining the axial power profile of partly flooded fuel in a compact core assembled in reactor LR-0, Ann. Nucl. Energy **90**, 450 (2016).
[38] M. Košťál *et al.*, Measurement and calculation of fast neutron and γ spectra in well defined cores in LR-0 reactor, Appl. Radiat. Isot. **120**, 45 (2017).
[39] M. Košťál *et al.*, Validation of zirconium isotopes (n, g) and (n, 2n) cross sections in a comprehensive LR-0 reactor operative parameters set, Appl. Radiat. Isot. **128**, 92 (2017).
[40] M. Kostal, M. Koštál, M. Švadlenková, P. Baroň, J. Milčák, M. Mareček, and J. Uhlíř, Measurement of ^{23}Na(n, 2n) cross section in well defined reactor spectra, App. Rad. Isot. **111**, 1 (2016).
[41] M. Kostal *et al.*, VVER-1000 physics experiments hexagonal lattices (1.275 cm Pitch) of low enriched U (3.3 wt.% ^{235}U)O_2 fuel assemblies in light water: ^{75}As(n, 2n), ^{23}Na(n, 2n), ^{90}Zr(n, 2n), ^{89}Y(n, 2n) reaction rates, in *International Handbook of Evaluated Reactor Physics Benchmark Experiments, Nuclear Energy Agency* (Paris, France, 2019).
[42] M. Kostal *et al.*, Validation of IRDFF-II library in VR-1 reactor field using thin targets, App. Rad. Isot. **158**, 108268 (2021).
[43] M. Koleska, M. Šunka, and J. Ernest, Validation of the on-site used operational code against burnup measurement, Nucl. Energy Radiat. Sci. **3**, 014502 (2017).
[44] M. Schulc, M. Koštál, E. Novák, R. Kubín, and J. Šimon, Application of ^{252}Cf neutron source for precise nuclear data experiments, Appl. Radiat. Isot. **151**, 187 (2019).
[45] M. Kostal *et al.*, Measurement of high energy gamma spectrum up to 13 MeV in the special core of the LR-0 reactor, in *Proceedings of International Conference on Physics of Reactors* (PHYSOR, San Francisco, USA, 2024).
[46] T. Czakoj *et al.*, Measurement of total fission gamma spectrum of ^{252}Cf(sf) (unpublished).
[47] A. J. Koning, D. Rochman, J. Sublet, N. Dzysiuk, M. Fleming, and S. van der Marck, TENDL: Complete nuclear data library for innovative nuclear science and technology, Nucl. Data Sheets **155**, 1 (2019).
[48] T. Goorley *et al.*, Initial MCNP6 release overview, Nucl. Tech. **180**, 298 (2012).
[49] www-nds.iaea.org/IRDFFtest/irdff_sp_Cf252_ln.dat.

Correction: The previously published Figures 2 and 3 contained errors in the legends and were missing data points and have been replaced. Corresponding errors have been fixed in text and in Tables I and II with clarifications made in the captions.